# IDENTIFICATION OF COMPLEX STRUCTURES USING NEAR-RESONANCE TESTING

By John P. Raney

NASA Langley Research Center
Langley Station, Hampton, Va.



Presented at the 38th Shock and Vibration Symposium

St. Louis, Missouri
May 1 and 2, 1968

# IDENTIFICATION OF COMPLEX STRUCTURES USING NEAR-RESONANCE TESTING

By J. P. Raney
NASA-Langley Research Center
Langley Station, Hampton, Virginia

## ABSTRACT

A recent innovation for determining the set of governing differential equations of motion of a complex structure is described. Numerical values for the mass, stiffness, and damping coefficients of the dynamical equations associated with a particular input-response or transmission path are computed from the data usually obtained in conventional vibration tests of a structure. The theory is based on the dynamic properties of multi-degree-of-freedom linear systems. The method requires the steady response (acceleration, velocity, displacement, or stress) and the driving sinusoidal force input for transmission paths of interest to be experimentally determined for a few frequencies near each major structure resonance. Application of the method is illustrated by determining from experimental data the equations of motion of 1/10- and 1/40-scale models of the Apollo/Saturn V launch vehicle. Transient responses computed using the identified equations for the 1/40-scale model are shown to agree favorably with experimental results.

## INTRODUCTION

The purpose of this paper is to present a simple technique for experimentally determining an acceptable set of equations of motion for a space vehicle structure. This system identification approach, while yielding the equations of motion, does not involve a detailed analysis or physical idealization of the structure. It relies solely on the experimental determination of the steady state response of the structure to a sinusoidally varying input force for a few frequencies near each important structural resonance and on the usual assumptions regarding the behavior of lightly damped, linear structures.

## SYMBOLS

| | |
|---|---|
| $[M]$ | system mass matrix; symmetric, positive definite |
| $[C]$ | system viscous damping matrix; symmetric, nonnegative definite |
| $[K]$ | system stiffness matrix; symmetric, nonnegative definite |
| $\{F(t)\}$ | system forcing function vector |
| $\{X\}$ | system coordinate vector |
| $x_k$ | $k^{th}$ system coordinate; an element of $\{X\}$ |
| $X_k$ | amplitude of steady state displacement response at $k$ |
| $\{X\}^{(j)}$ | system coordinate vector due only to response in the $j$th mode |
| $x_k^{(j)}$ | kth element of $\{X\}^{(j)}$ |
| $[\Psi]$ | matrix of modal vectors $\{\varphi\}^{(j)}$ as columns |
| $\{\varphi\}^{(j)}$ | modal vector obtained from $\left[[K] - \lambda_j[M]\right]\{X\} = 0$ |
| $\varphi_i^{(j)}, \varphi_k^{(j)}$ | the ith and kth elements of $\{\varphi\}$ |
| $[\overline{M}]$ | diagonal modal mass matrix |
| $[\overline{C}]$ | diagonal modal damping matrix |
| $[\overline{K}]$ | diagonal modal stiffness matrix |
| $\{q\}$ | normal coordinates defined by $\{X\} = [\Psi]\{q\}$ |
| $q_j$ | jth element of $\{q\}$ |
| $m_j, c_j, k_j$ | jth modal mass, damping and stiffness |
| $F_i(t)$ | arbitrary external point force applied at $i$ |
| $F_i$ | amplitude of $F_i \sin\omega t$ |
| $m_{ik}^{(j)}, c_{ik}^{(j)}, k_{ik}^{(j)}$ | effective mass, damping and stiffness for the i–k input–output path in the jth mode |
| $\theta_{ik}$ | phase angle between response and input force for the i–k path |
| $\mu_{ik}^{(j)}$ | effective percent of critical damping in the jth mode |
| $\omega$ | circular frequency |

| | |
|---|---|
| $\omega_j$ | jth resonant circular frequency |
| Units | the units used in this paper are lb, in, sec |

## THEORY

The starting point for the development of the identification technique of this paper is in the mechanics of lightly damped, linear systems. The class of structures for which the technique is proposed is assumed to possess the following somewhat qualitative features which are stated in the form of assumptions and are basic to the ensuing development:

1. Light damping typical of a space vehicle with no damping specifically designed into the structure.
2. The modes of interest are sufficiently uncoupled in the velocity terms and separated in frequency so that a single degree-of-freedom analysis is adequate to represent the steady response above the half power point in a mode of interest.

These basic assumptions are designed to imply that the steady response in each vibration mode of interest is not significantly affected by any other mode and that each mode can be isolated and individually exploited as discussed in detail in references (1) – (4).

With the above assumptions as a background, the proposed identification technique and the supporting analytical arguments are now developed.

General. – The equations of motion for the system may be written (ref. 5)

$$[M]\{\ddot{X}\} + [C]\{\dot{X}\} + [K]\{X\} = \{F(t)\} \qquad (1)$$

The transformation

$$\{X\} = [\Psi]\{q\} \tag{2}$$

where

$$x_k = \sum_j \varphi_k^{(j)} q_j \tag{3}$$

is assumed to produce uncoupled equations in terms of the normal coordinates, q, so that

$$[\overline{M}]\{\ddot{q}\} + [\overline{C}]\{\dot{q}\} + [\overline{K}]\{q\} = [\Psi]^T\{F(t)\} \tag{4}$$

where

$$[\overline{M}] = [\Psi]^T[M][\Psi]$$

$$[\overline{C}] = [\Psi]^T[C][\Psi]$$

$$[\overline{K}] = [\Psi]^T[K][\Psi]$$

The equation for the jth normal coordinate is

$$m_j\ddot{q}_j + c_j\dot{q}_j + k_jq_j = \sum_i \varphi_i^{(j)} F_i(t) \tag{5}$$

For only one external forcing function applied at i equation (5) becomes

$$m_j\ddot{q}_j + c_j\dot{q}_j + k_jq_j = \varphi_i^{(j)} F_i(t) \tag{6}$$

Near resonant response. – Equation (2) may be written

$$\{X\} = \sum_j \{\varphi\}^{(j)} q_j$$

so that the response in the jth mode is

$$\{X\}^{(j)} = \{\varphi\}^{(j)} q_j \tag{7}$$

or

$$x_k^{(j)} = \varphi_k^{(j)} q_j \tag{8}$$

and

$$q_j = \frac{x_k^{(j)}}{\varphi_k^{(j)}} \tag{9}$$

Substituting equation (9) into equation (6) and dividing by $\varphi_i^{(j)}$

$$\left( \frac{m_j}{\varphi_i^{(j)} \varphi_k^{(j)}} \right) \ddot{x}_k^{(j)} + \left( \frac{c_j}{\varphi_i^{(j)} \varphi_k^{(j)}} \right) \dot{x}_k^{(j)} + \left( \frac{k_j}{\varphi_i^{(j)} \varphi_k^{(j)}} \right) x_k^{(j)} = F_i(t) \tag{10}$$

or

$$m_{ik}^{(j)} \ddot{x}_k^{(j)} + c_{ik}^{(j)} \dot{x}_k^{(j)} + k_{ik}^{(j)} x_k^{(j)} = F_i(t) \tag{11}$$

The significance of equation (11) is that it represents the system dynamics for response at point k due to forcing at point i. Also, the derivation of equation (11) has not placed any restrictions on the forcing function at i. $F_i(t)$ is, in fact, an arbitrary, external, point forcing function. When $F_i(t) = F_i \sin \omega t$ with $\omega = \omega_j$ only one equation of the form of equation (11) is required to represent the system response. It is upon this fact that the identification scheme is based.

Equating the coefficients of equations (10) and (11), it is evident that

$$\begin{aligned} m_j &= m_{ik}^{(j)} \varphi_i^{(j)} \varphi_k^{(j)} \\ c_j &= c_{ik}^{(j)} \varphi_i^{(j)} \varphi_k^{(j)} \\ k_j &= k_{ik}^{(j)} \varphi_i^{(j)} \varphi_k^{(j)} \end{aligned} \tag{12}$$

Setting $i = k$

$$m_j = m_{ii}^{(j)}[\varphi_i^{(j)}]^2 \tag{13}$$

from which the modal amplitudes at $i$ and $k$ are found to be given by

$$\varphi_i^{(j)} = \sqrt{\frac{m_j}{m_{ii}^{(j)}}}$$

$$\varphi_k^{(j)} = \frac{m_j}{m_{ik}^{(j)}\varphi_i^{(j)}} \tag{14}$$

The quantities $m_j$ and $m_{ii}^{(j)}$ are defined to be positive and hence $\varphi_i^{(j)}$ is positive. A negative value for $\varphi_k^{(j)}$ implies a negative $m_{ik}^{(j)}$ which is wholly consistent with the facts.

Solutions for $m_{ik}$, $c_{ik}$, and $k_{ik}$. – The steady state or particular solution of equation (11) with $F_i(t) = F_i \sin\omega t$ is given by

$$x = X \sin(\omega t - \theta) \tag{15}$$

Substituting equation (15) into equation (11) and solving for the coefficients $m_{ik}$, $c_{ik}$ and $k_{ik}$ results in

$$k_{ik}^{(j)} = m_{ik}^{(j)}\omega^2 + \frac{F_i}{X_k}\cos\theta_{ik} \tag{16}$$

and

$$c_{ik}^{(j)} = \frac{F_i}{\omega X_k}\sin\theta_{ik} \tag{17}$$

If one set of values of $\omega$, $F_i$, $X_k$ and $\theta_{ik}$ for equation (17) and two sets for equation (16) are known, the coefficients of equation (11) may be computed.

Response to Arbitrary Force. – The total system response at $k$ due to any time dependent force $F_i(t)$ at $i$ is found by superposition of the solutions of each of the set of the following equations:

$$\begin{aligned}
m_{ik}^{(1)}\ddot{x}_k^{(1)} + c_{ik}^{(1)}\dot{x}_k^{(1)} + k_{ik}^{(1)}x_k^{(1)} &= F_i(t) \\
\vdots \qquad\qquad \vdots \qquad\qquad \vdots \qquad\qquad &\vdots \\
m_{ik}^{(j)}\ddot{x}_k^{(j)} + c_{ik}^{(j)}\dot{x}_k^{(j)} + k_{ik}^{(j)}x_k^{(j)} &= F_i(t) \\
\vdots \qquad\qquad \vdots \qquad\qquad \vdots \qquad\qquad &\vdots \\
m_{ik}^{(p)}\ddot{x}_k^{(p)} + c_{ik}^{(p)}\dot{x}_k^{(p)} + k_{ik}^{(p)}x_k^{(p)} &= F_i(t)
\end{aligned} \tag{18}$$

and is given using equations (3) and (8) as

$$x_k = \sum_{j=1}^{p} x_k^{(j)}$$

## EXPERIMENTAL PROCEDURE

The Langley 1/10-scale and 1/40-scale models of the Apollo/Saturn V launch vehicle are shown in figures 1 and 2 and the coordinate systems for both models are presented in figure 3. The 1/10-scale model is fully described in reference 6.

1/10-scale model. – The 1/10-scale model was complete in the lift-off structural configuration, but was entirely empty of simulated propellants. The boundary conditions were cantilevered-free. A steady frequency, transverse, sinusoidally varying input force was applied in the pitch plane through a strain gage type force gage at station 386 and the displacements at stations 418 (the tip of the escape tower), 377, and 282 were measured using a contacting, cantilever, strain gage beam. The strain gage displacement transducers had natural frequencies in the order of 60 cps and were used within their flat response regime. The signals from the force and the displacement transducers were processed through a balancing bridge, differential amplifier, D.C. isolation amplifier and were then recorded together with the calibration signals on an FM analog tape recorder. The selection of both strain gage force and displacement transducers with both signals processed through identical electronics was to assure the accurate determination of phase angle, $\theta_{ik}$, for use in equations (16) and (17).

1/40-scale model. – The 1/40-scale model was also complete in the lift-off structural configuration. Propellant loading corresponded to first stage burnout and the boundary conditions simulated were free-free. A steady frequency transverse, sinusoidally varying input force was applied in the

pitch plane through a crystal type force gage alternately at stations 0 and 42 and the acceleration responses were measured at model stations 102.9 and −2.7. The crystal transducers were used with this model in order to evaluate the quality of data produced by the two different instrumentation schemes. The signals from the force gage and accelerometers were processed through similar conditioning equipment to minimize relative phase shift and, together with calibration signals, were recorded on tape.

Data reduction. – The experimental analog data were digitally filtered using a 24–point per cycle Fourier analysis from which the numerical amplitudes of the fundamental components of the input force and of the displacement and acceleration responses and the input–response phase angles, $\theta_{ik}$, were computed.

## IDENTIFICATION PROCEDURE

### System Equations

For convenience equations (18) were written as

$$\begin{aligned} \ddot{x}_k^{(1)} + 2\mu_{ik}^{(1)}\omega_1\dot{x}_k^{(1)} + \omega_1^2 x_k^{(1)} &= \frac{1}{m_{ik}^{(1)}}F_i(t) \\ \vdots \qquad\qquad \vdots \qquad\qquad \vdots \qquad\qquad &\vdots \\ \ddot{x}_k^{(p)} + 2\mu_{ik}^{(p)}\omega_p\dot{x}_k^{(p)} + \omega_p^2 x_k^{(p)} &= \frac{1}{m_{ik}^{(p)}}F_i(t) \end{aligned} \tag{19}$$

and

$$x_k = \sum_{j=1}^{p} x_k^{(j)} \tag{20}$$

Computer experiments. – A controlled computer experiment was conducted in which an exact numerical solution of equations (19) and (20) was generated for an assumed set of typical coefficients. The solution was then corrupted and the coefficients $m_{ik}^{(j)}$, $c_{ik}^{(j)}$, and $k_{ik}^{(j)}$ were computed using equations (16) and (17). The results indicated that errors of up to $\pm$ 10 percent in $F_i/X_k$ and $\pm$ 10 degrees in $\theta_{ik}$ can be tolerated by this identifier when applied to systems which satisfy the basic assumptions of this paper. Since it was felt that the accuracy of the experimental data fell within these limits, identification of the 1/10-scale and 1/40-scale models was attempted.

Solution for coefficients. – The digitized experimental data, $F_i$, $x_k$ or $\ddot{X}_k$, $\theta_{ik}$ corresponding to a near resonant value of $\omega$ were used to determine the values of $m_{ik}^{(j)}$, $c_{ik}^{(j)}$, $k_{ik}^{(j)}$ for each significant mode for each of the selected input-response paths for each model. Four or five frequencies near each resonance were used. The value of $c_{ik}^{(j)}$ for each point was computed using equation (17). The values of $m_{ik}^{(j)}$ and $k_{ik}^{(j)}$ were determined by solving equation (16) as a pair of simultaneous equations for slightly different near-resonant values of $\omega$. The average value of effective mass, damping, and stiffness for each mode was then determined. Typical first mode values for station 377 response of the 1/10-scale model are as follows:

| Frequencies | | Coefficients of Eqn. | | | Coefficients of Eqn. | | |
|---|---|---|---|---|---|---|---|
| f | $\omega$ | $m_{ik}^{(1)}$ | $c_{ik}^{(1)}$ | $k_{ik}^{(1)}$ | $2\mu_{ik}\omega_1 = \frac{c_{ik}^{(1)}}{m_{ik}^{(1)}}$ | $\omega_1^2 = \frac{k_{ik}^{(1)}}{m_{ik}^{(1)}}$ | $\frac{1}{m_{ik}^{(1)}}$ |
| 4.52 | 28.39 | .3479 | .1458 | 304.9 | .4191 | 876.4 | 2.87 |
| 4.72 | 29.64 | .3381 | .1615 | 296.2 | .4777 | 876.7 | 2.96 |
| 4.99 | 31.34 | .3311 | .1611 | 290.1 | .4866 | 876.2 | 3.02 |

The sign of $m_{ik}^{(j)}$ computed using equation (16) was very simply verified. The sign was taken to be positive if $\varphi_k^{(j)}$ was in phase (approximately $0^o$) with $\varphi_i^{(j)}$ and negative if $\varphi_k^{(j)}$ was out of phase (approximately $180^o$) with $\varphi_i^{(j)}$. The identification results for both models are listed as coefficients of equation (19) in Tables I and II.

## RESULTS AND DISCUSSION

Comparisons of the identification and experimental frequency responses for the two models are presented in figures 4–10.

1/10-scale results.– The results for the 1/10-scale model are shown in figures 4–6, plotted as the response ratio $\left|\frac{X_k}{F_i}\right|$ versus frequency. The particular solutions of equations (19) were obtained for $F_i(t) = \sin\omega t$, i = station 386, for $0 \leq \frac{\omega}{2\pi} \leq 30$ using the coefficients listed in Table I.

The frequency response at stations 418, 377, and 282 were then obtained using equation (20). For example,

$$x_{418} = x_{418}^{(1)} + x_{418}^{(2)} + x_{418}^{(3)}$$

1/40-scale results. – The results for the 1/40-scale model are shown in figures 7–10. The frequency response solutions for forcing first at station 0 and then at station 42 were computed using equations (19) and (20) and the coefficients given in Table II. For example, for response at station 102.9 due to forcing at station 42

$$\ddot{x}_{102.9}^{(1)} + 3.14\dot{x}_{102.9}^{(1)} + 69{,}530x_{102.9}^{(1)} = -10.1 \sin\omega t$$

$$\ddot{x}_{102.9}^{(2)} + 4.54\dot{x}_{102.9}^{(2)} + 289{,}300x_{102.9}^{(2)} = 16.2 \sin\omega t$$

$$\ddot{x}_{102.9}^{(3)} + 13.71\dot{x}_{102.9}^{(3)} + 681{,}160x_{102.9}^{(3)} = -12.2 \sin\omega t$$

$$\ddot{x}_{102.9}^{(4)} + 26.25\dot{x}_{102.9}^{(4)} + 929{,}870x_{102.9}^{(4)} = -11.7 \sin\omega t$$

and

$$x_{102.9} = x_{102.9}^{(1)} + x_{102.9}^{(2)} + x_{102.9}^{(3)} + x_{102.9}^{(4)}$$

Discussion. – The identification results for both models agree quite favorably with the experimental response data. In addition, the associated phase angles, $\angle \frac{X_k}{F_i}$, also agree, usually to within 5 to 10 degrees.

Therefore, it is felt that, for both models and for the input-response paths investigated, systems of equations suitable for computing the response to an arbitrary forcing function have been obtained.

In this connection, the uniqueness of the identified equations has not been rigorously established. It is, however, felt that amplitude agreement as shown in figures 4-10 together with phase agreement to within 5 to 10 degrees, constitutes sufficient conditions for a system identification adequate for all engineering purposes. The experience thus far also indicates, for the class of systems considered in this paper, that an identifier based on requiring coincidence of frequency response amplitudes only, without regard to phase, will produce basically the same results as if phase information were employed. This fact can be useful, because, in general, some obvious small adjustments of the identified parameters to give better results based on amplitude comparison is usually possible. Figures 4-10 as presented indicate the results that were achieved using the method of this paper without iteration. However, parameters were easily selected to produce perfect coincidence of the amplitude plots of both figures 8 and 10, for example. The phase differences were negligible. Therefore, it is felt that refinement of the identified equations to produce perfect amplitude agreement is permissable, if not desirable.

The advantages of using the approach of this paper are that a detailed structural idealization and associated analytical model is not required. The modes that actually contributed to the response were immediately identified as the only ones observable for a given input response path. This

obviated the usual concern over the problem of including all of the significant vibratory modes of the structures.

Once the equations of motion for a structure have been identified the transient response to an arbitrary force can be computed with confidence. In this connection, rigid body modes, if required, can be calculated from model drawings or experimentally determined. Results thus far of transient tests with the 1/40-scale model have produced excellent agreement between the acceleration response computed using the identified equations and the experimental transient acceleration responses. For example, a comparison of identification and experimental transient acceleration and displacement responses for the 1/40-scale model is shown in figure 11(a) and (b). The coefficients used in computing the acceleration response as predicted using the system identification results are given in Table II for $i = 0$ and $k = 102.9$ (see figure 7). In addition, the two rigid body modes required for this free-free system were included which resulted in five equations of motion which were integrated using the measured values of the transient input shown in figure 11(c) which was applied at station 0 of the model. The identified equations predict transient acceleration and displacement responses at station 102.9 which are in good agreement with the experimentally determined response. The results of figure 11 are especially important because they demonstrate the ability of the identified equations to predict accurately the response to an input of a different character than was used for their derivation.

## CONCLUDING REMARKS

A technique for determining the equations of motion of a complex structure has been presented. Both the number of the essential degrees of freedom and the coefficients of the equations are determined by the procedure which is applicable to a large class of aerospace and other structures. The procedure requires that good quality experimental frequency response data be obtained for the significant resonances associated with specified input response paths.

It is felt, for the class of structures considered in this paper, that coincidence of the identified and experimental frequency response amplitudes constitutes a sufficient condition for a satisfactory identification. This hypothesis, if true, suggests that refinement of the initial identification results to produce perfect amplitude agreement is desirable and may be useful in the formulation of an identifier that does not require explicit experimental phase information.

It is felt that this identification procedure should be advantageous when the dynamical equations of motion for an existing structure are desired. For example, if the available resources are not sufficient to allow the formulation and verification of a detailed analytical model of an existing structure, of if only sinusoidal test equipment is available but transient response data are required, the procedure of this paper may be very useful. In particular, the identified equations were shown adequately to predict the system acceleration response to an arbitrary transient force.

## REFERENCES


1. Plunkett, R.: Semi-Graphical Method for Plotting Vibration Response Curves. Proc. Second U.S. Cong. of Applied Mech. pp. 121-126, 1954.

2. Thorn, Richard P.; and Church, Austin H.: Simplified Vibration Analysis by Mobility and Impedance Methods. Reprinted from Machine Design. The Penton Publishing Company. 1960.

3. Raney, J. P.: Analog Computer Solution for Transverse Vibrations of a Uniform Beam with Damped, Flexible, Massive End Restraints. Developments in Theoretical and Applied Mechanics, Vol. 1, Plenum Press, 1963.

4. Howlett, J. T.; and Raney, J. P.: New Approach for Evaluating Transient Loads for Environmental Testing of Spacecraft. The Shock and Vibration Bulletin, Bul. 36, Part 2, pp. 97-105, January 1967.

5. Caughey, T. K.; and O'Kelley, M. E. J.: Classical Normal Modes in Damped Linear Systems. J. of Applied Mechanics, Vol. 32, Series E, No. 3, pp. 583-588, September 1965.

6. Leadbetter, Sumner A.; Leonard, H. Wayne; and Brock, E. John, Jr.: Design and Fabrication Considerations for a 1/10-Scale Replica Model of the Apollo/Saturn V. NASA TN D-4138, 1967.

TABLE I.- IDENTIFIED VALUES OF THE COEFFICIENTS OF EQUATION (19) FOR 1/10-SCALE MODEL

All Stages Empty, Cantilevered-free

| Station, k | | 418 | | 377 | | 282 | |
|---|---|---|---|---|---|---|---|
| Mode, j | 1 | 2 | 3 | 1 | 2 | 1 | 2 |
| $2\mu_{ik}^{(j)}\omega_j$ | .472 | 4.19 | 15.4 | .477 | 3.40 | .479 | 2.85 |
| $\omega_j^2$ | 877 | 9,240 | 28,360 | 876 | 8,860 | 877 | 9,350 |
| $\frac{1}{m_{ik}^{(j)}}$ | 3.89 | 9.01 | -4.85 | 2.95 | 2.30 | 1.39 | -1.93 |

TABLE II. – IDENTIFIED VALUES OF THE COEFFICIENTS OF EQUATION (19) FOR 1/40-SCALE MODEL

First Stage Empty, Free-Free

Force at Station 0

| | | | | | | | |
|---|---|---|---|---|---|---|---|
| Station, k | | 102.9 | | | | −2.7 | |
| Mode, j | 1 | 2 | 3 | 1 | 2 | 3 | |
| $2\mu_{ik}{}^{(j)}\omega_j$ | 4.00 | 6.76 | 13.90 | 2.76 | 5.20 | 60.0 | |
| $\omega_j^2$ | 68,900 | 288,000 | 683,000 | 69,000 | 288,000 | 680,000 | |
| $\frac{1}{m_{ik}^{(j)}}$ | 39.0 | −28.8 | 10.1 | 6.87 | 3.24 | 10.2 | |

Force at Station 42

| | | | | | | | | |
|---|---|---|---|---|---|---|---|---|
| Station, k | | 102.9 | | | | −2.7 | | |
| Mode, j | 1 | 2 | 3 | 4 | 1 | 2 | 3 | 4 |
| $2\mu_{ik}{}^{(j)}\omega_j$ | 3.14 | 4.54 | 13.71 | 26.25 | 4.2 | 2.68 | 30.60 | 20.12 |
| $\omega_j^2$ | 69,530 | 289,300 | 681,160 | 929,870 | 69,700 | 287,100 | 691,650 | 933,400 |
| $\frac{1}{m_{ik}^{(j)}}$ | −10.1 | 16.2 | −12.2 | −11.7 | −2.82 | −2.25 | −1.37 | −9.00 |

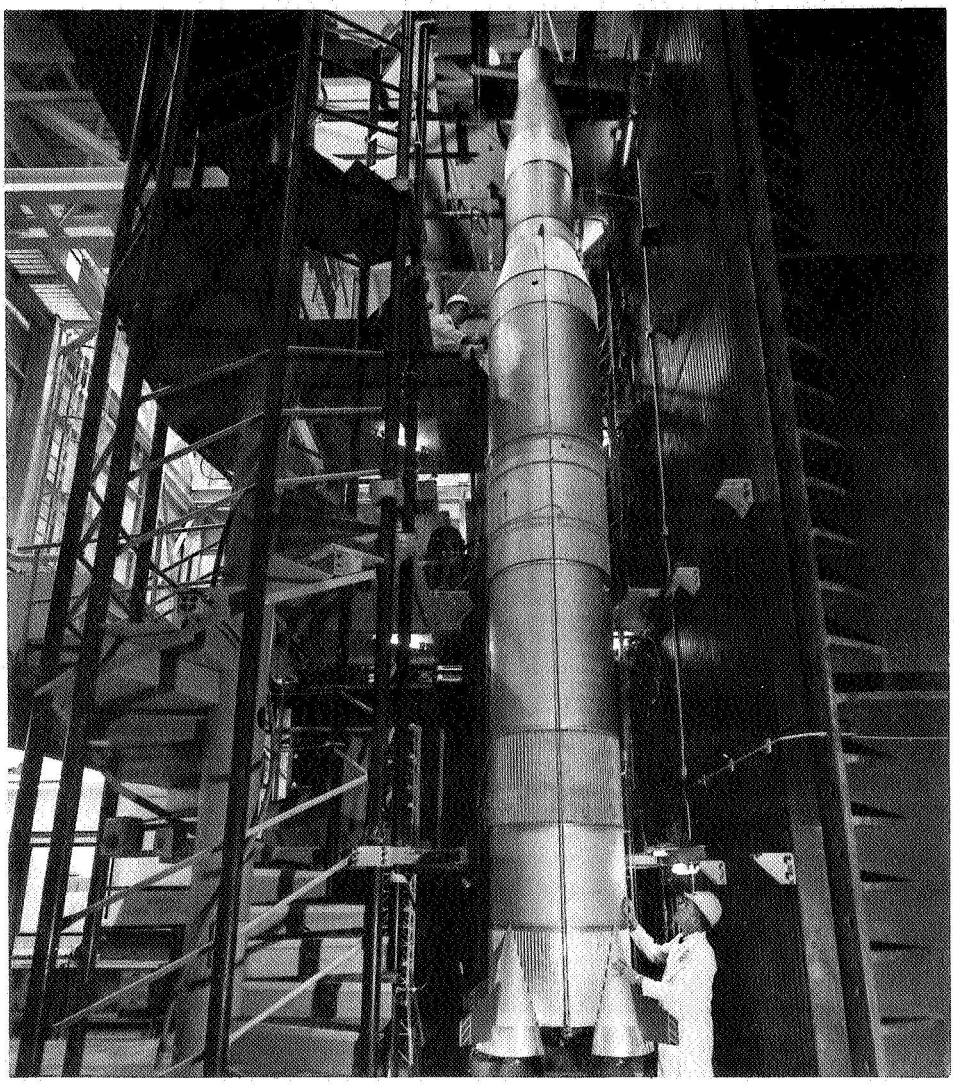

Figure 1.- 1/10-scale Apollo/Saturn V model.

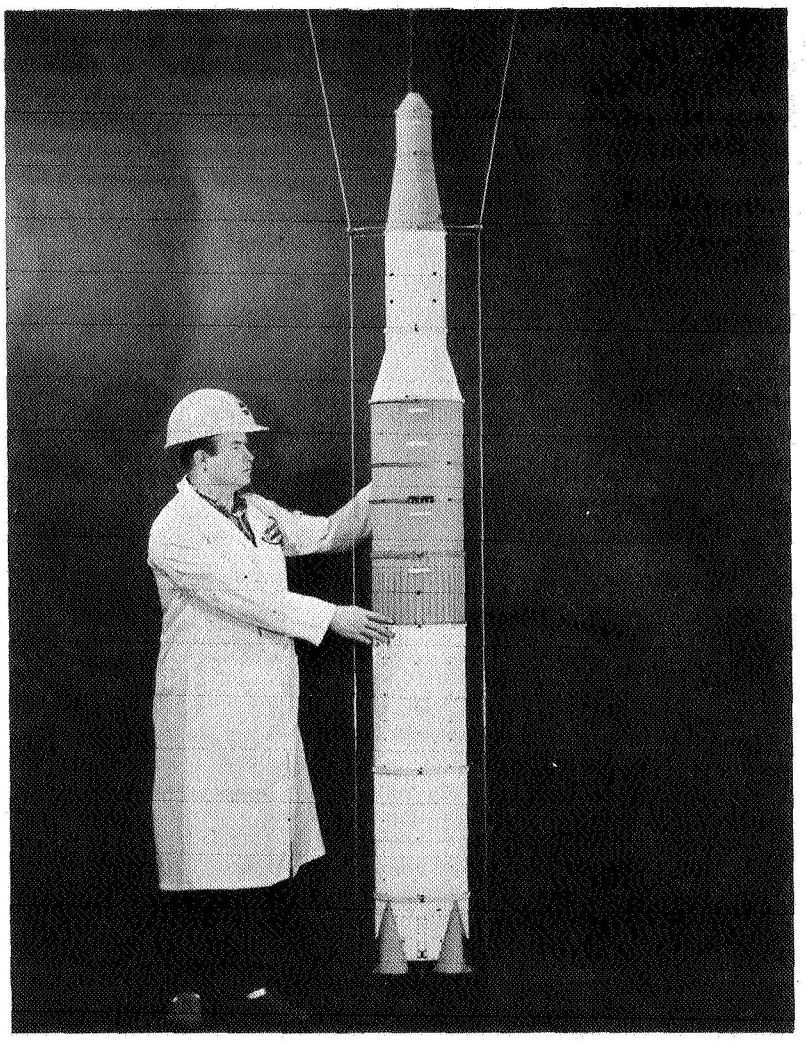

Figure 2.- 1/40-scale Apollo/Saturn V model.

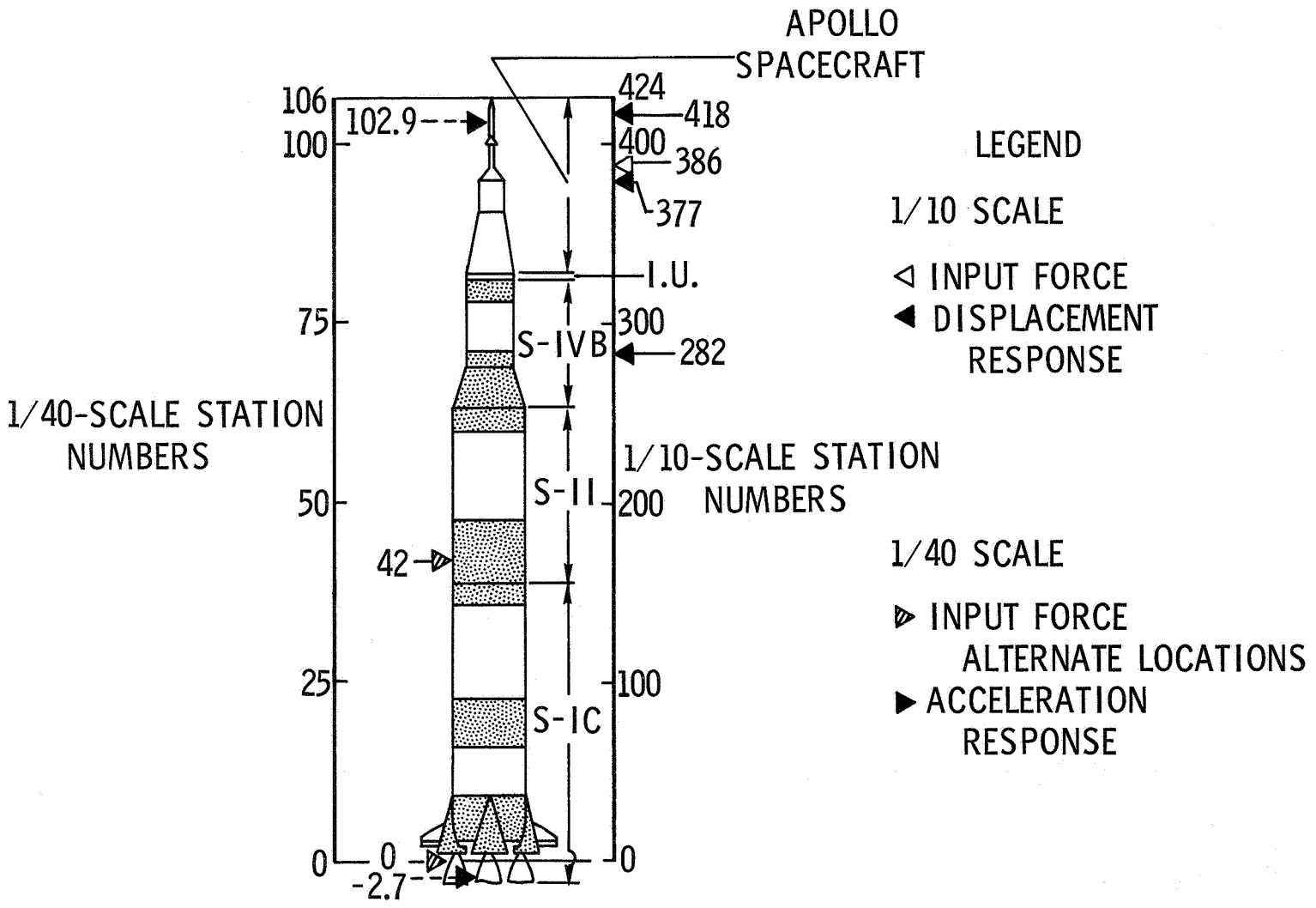


Figure 3.- Schematic of Apollo/Saturn V models.

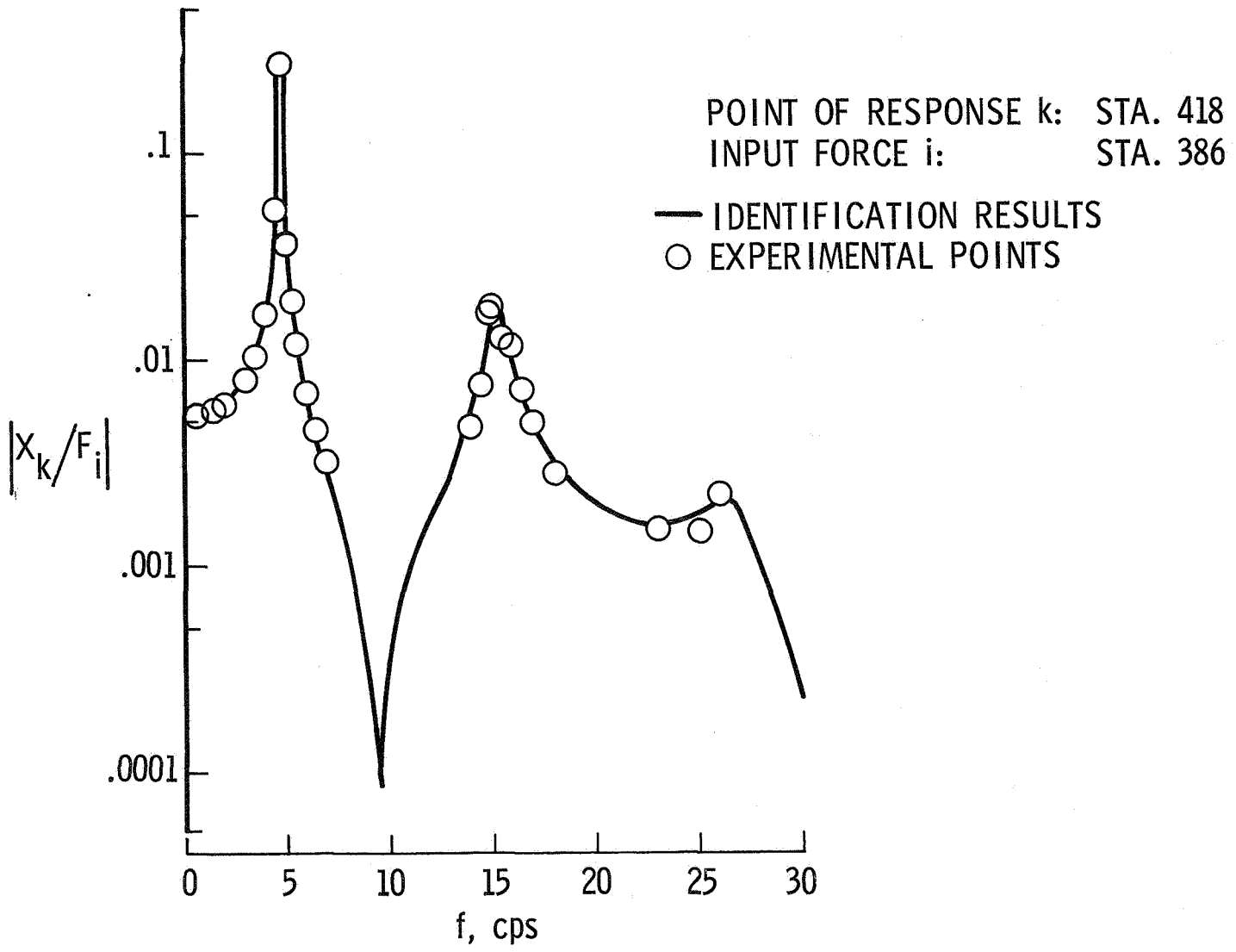


Figure 4.- Comparison of identification results with experimental frequency response for 1/10-scale model.

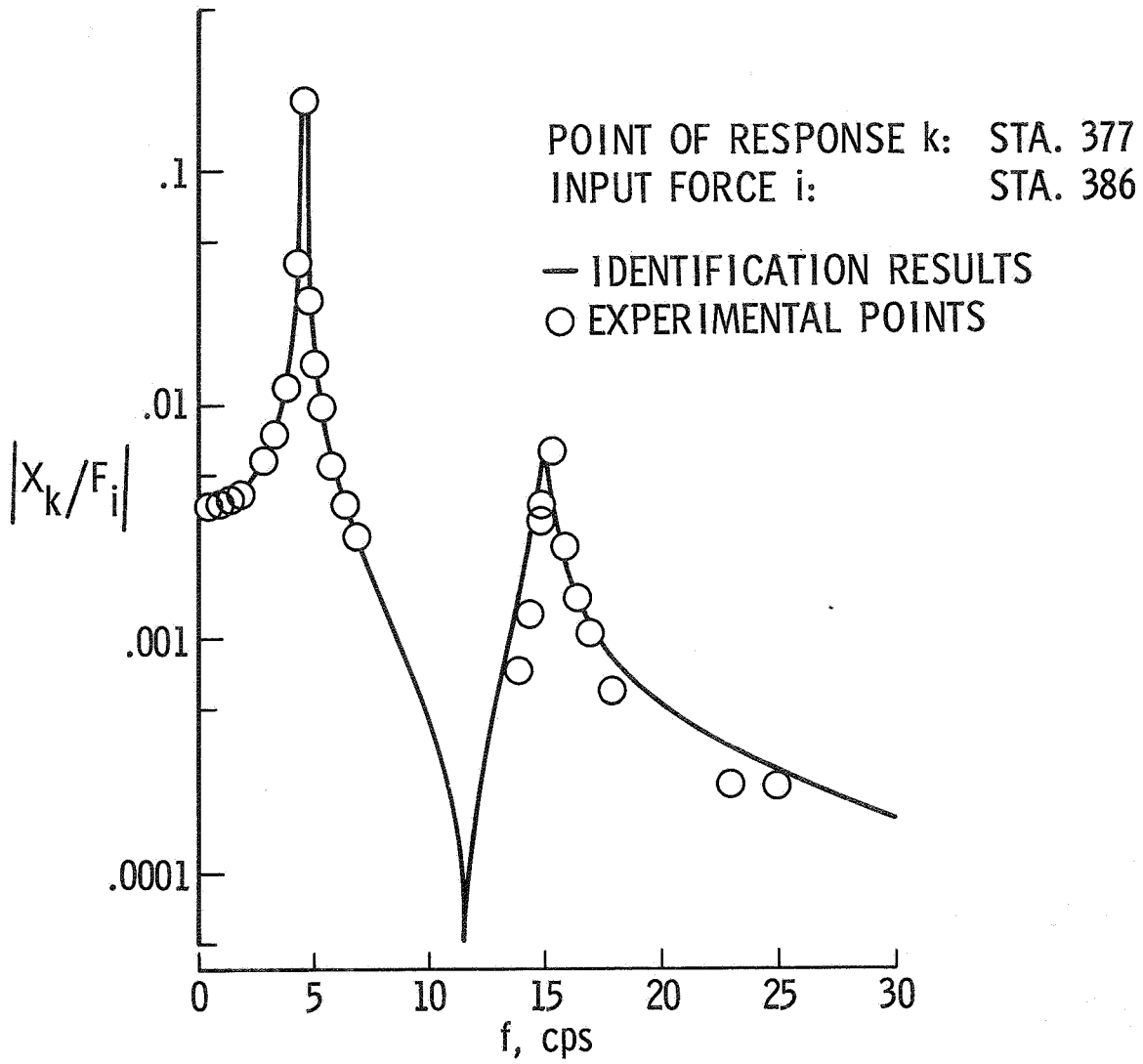


Figure 5.- Comparison of identification results with experimental frequency response for 1/10-scale model.

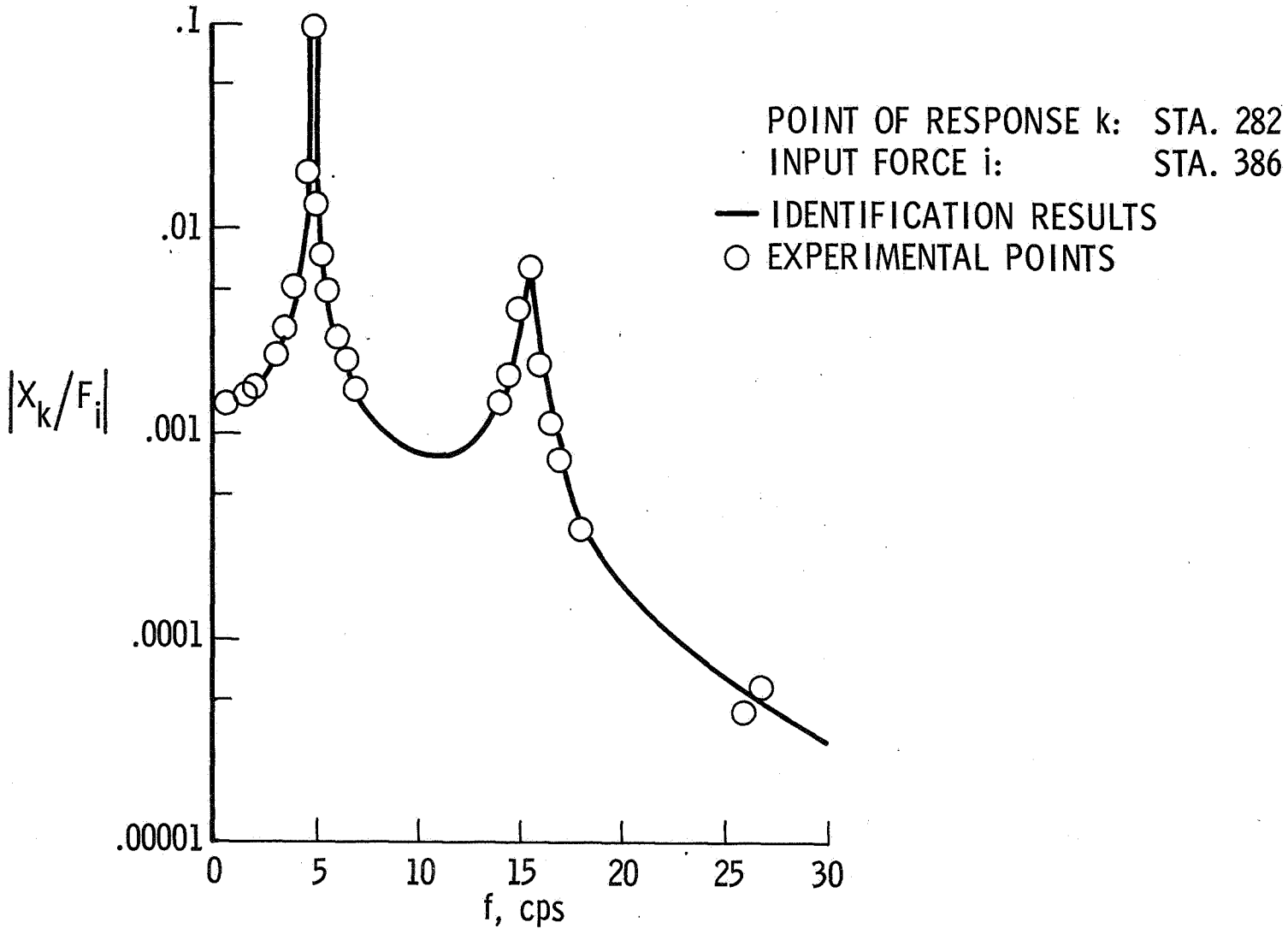


Figure 6.- Comparison of identification results with experimental frequency response for 1/10-scale model.

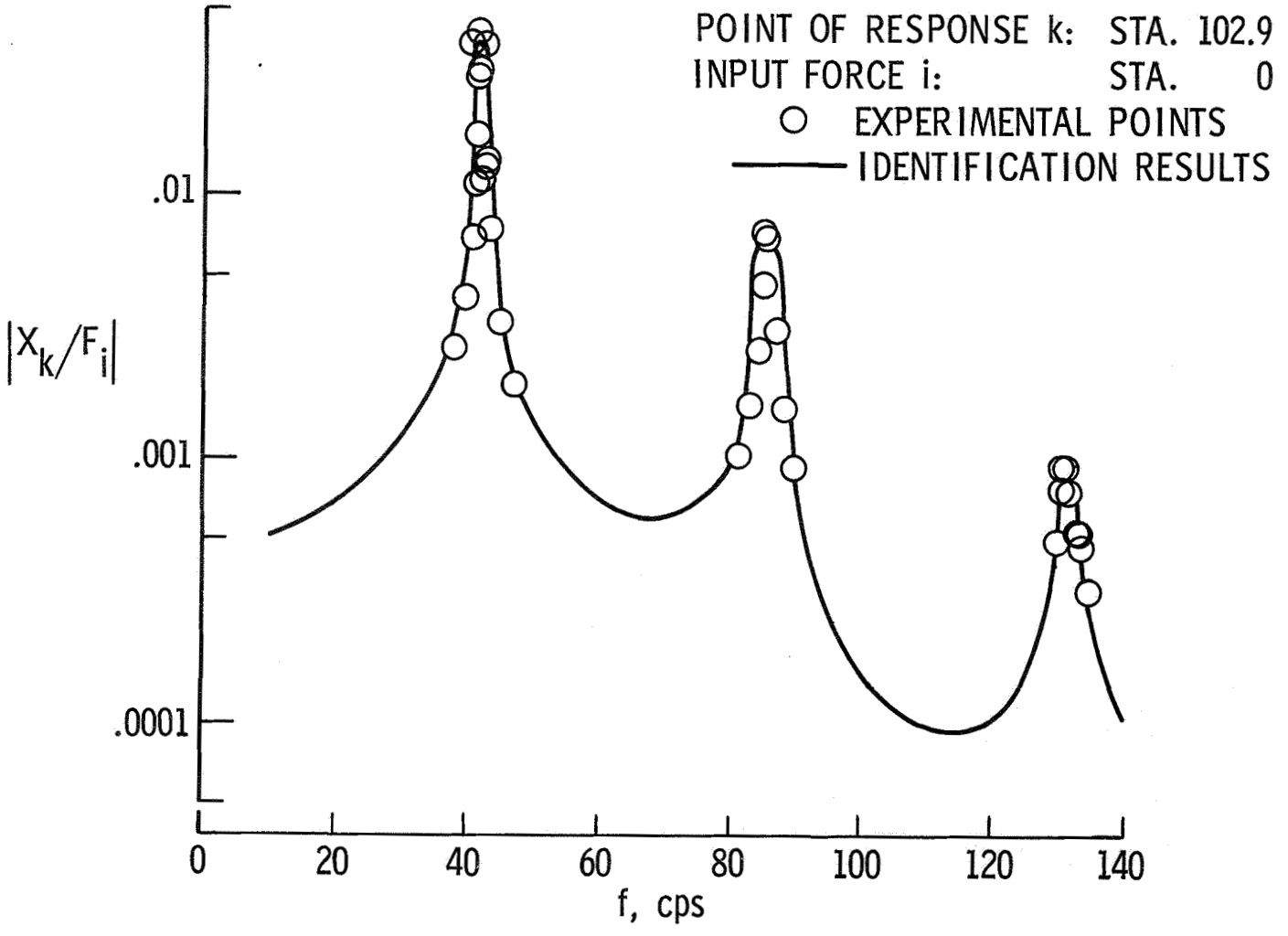


Figure 7.- Comparison of identification results with experimental frequency response for 1/40-scale model.

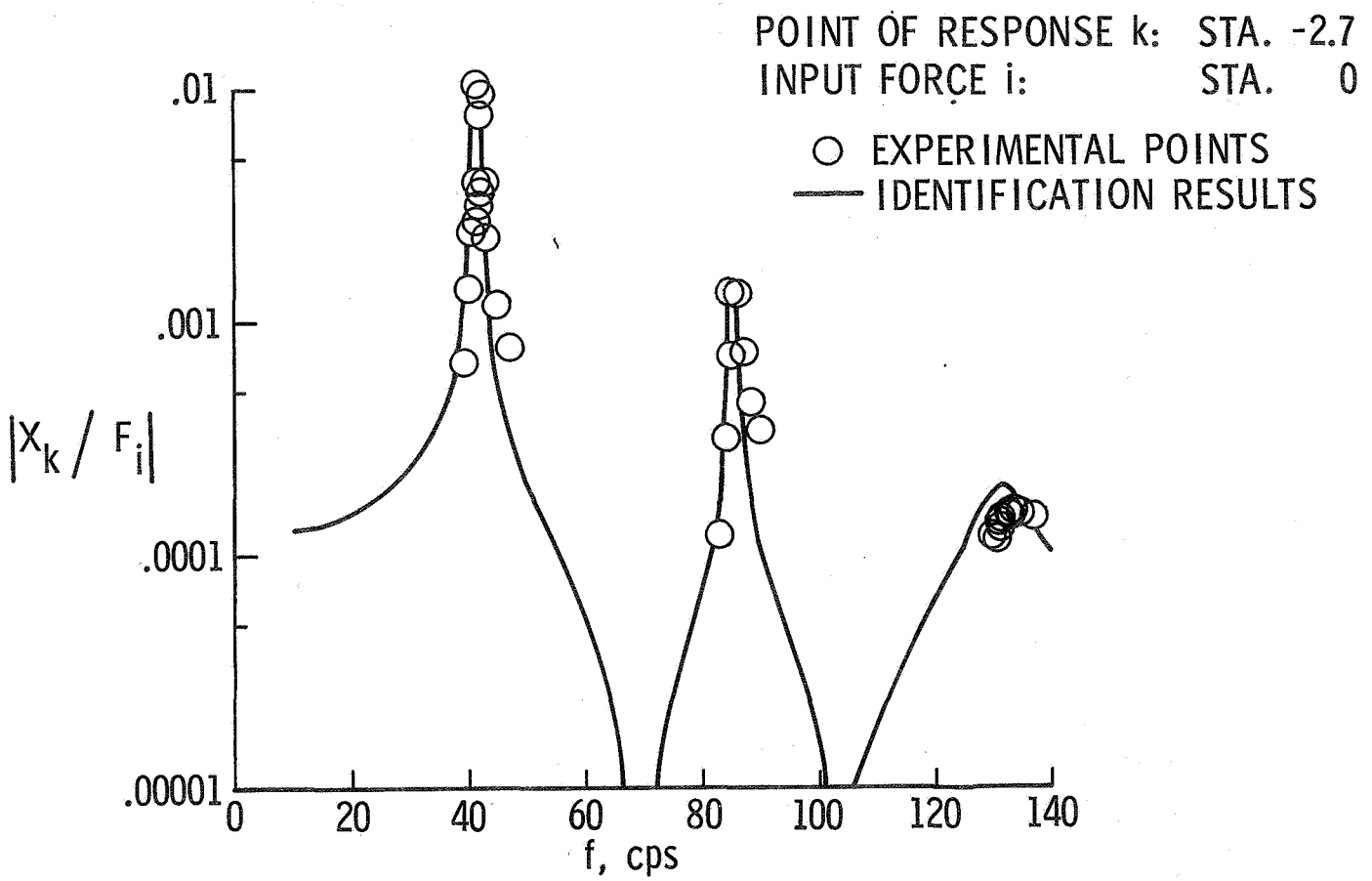


Figure 8.- Comparison of identification results with experimental frequency response for 1/40-scale model.

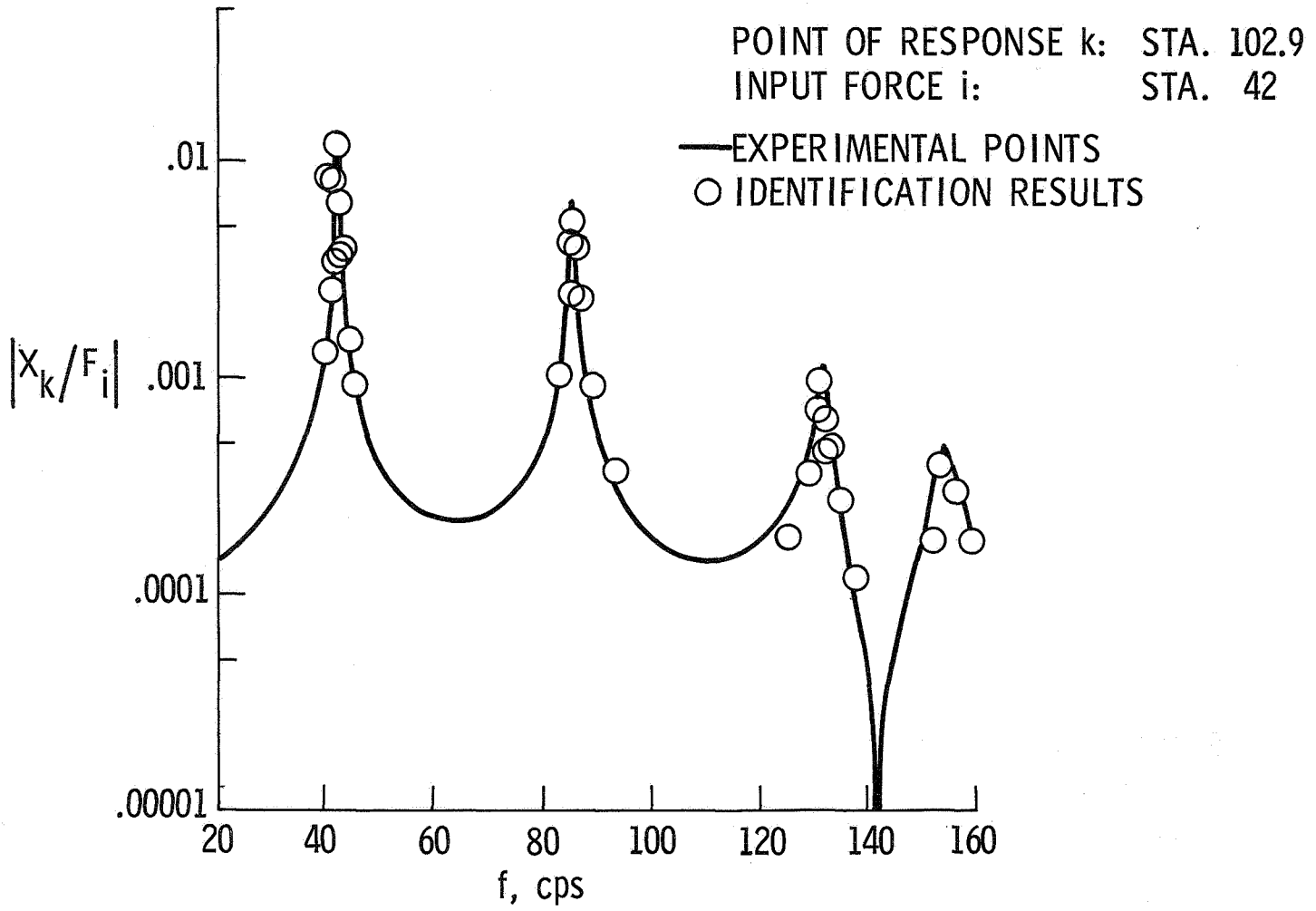


Figure 9.- Comparison of identification results with experimental frequency response for 1/40-scale model.

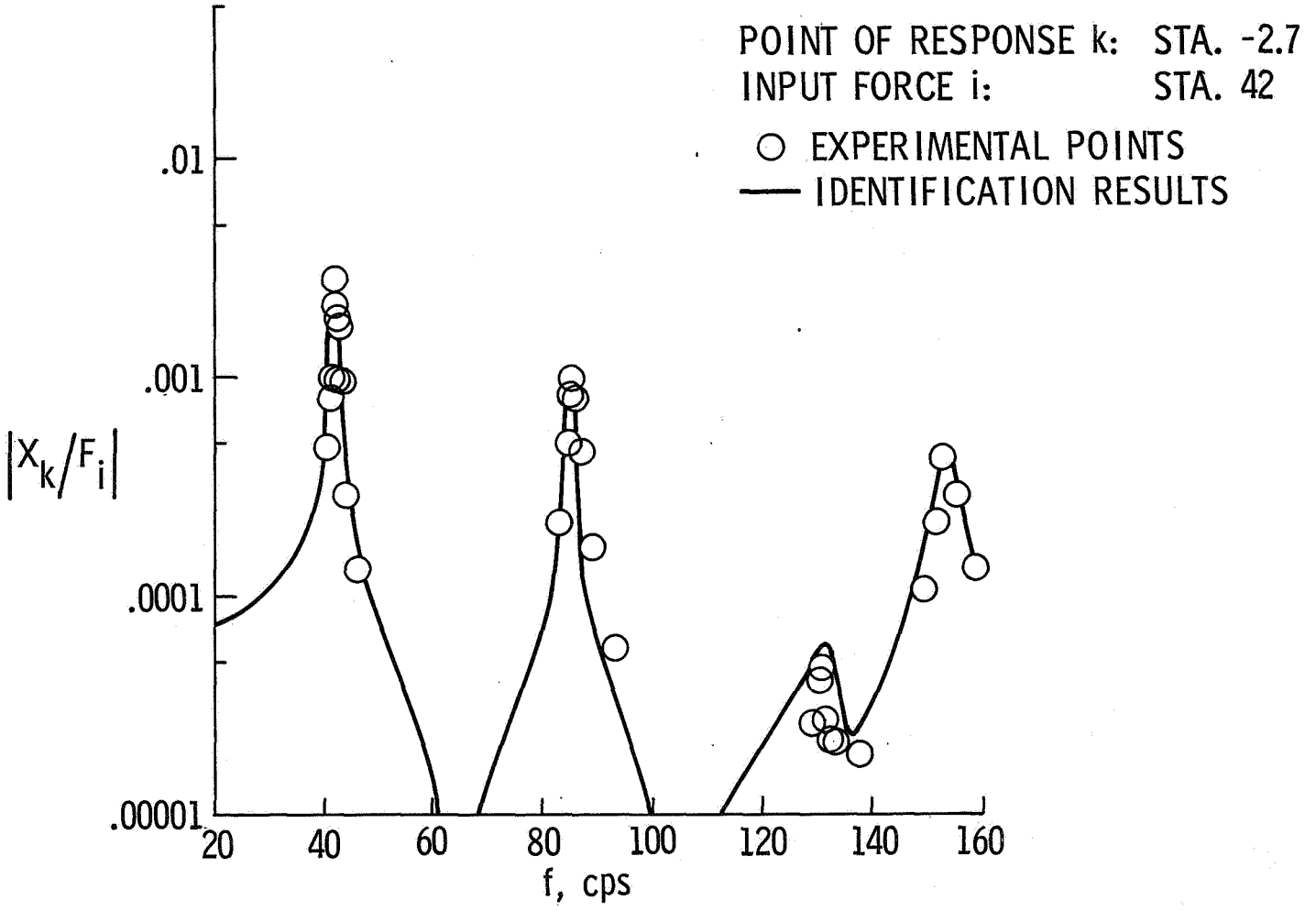


Figure 10.- Comparison of identification results with experimental frequency response for 1/40-scale model.

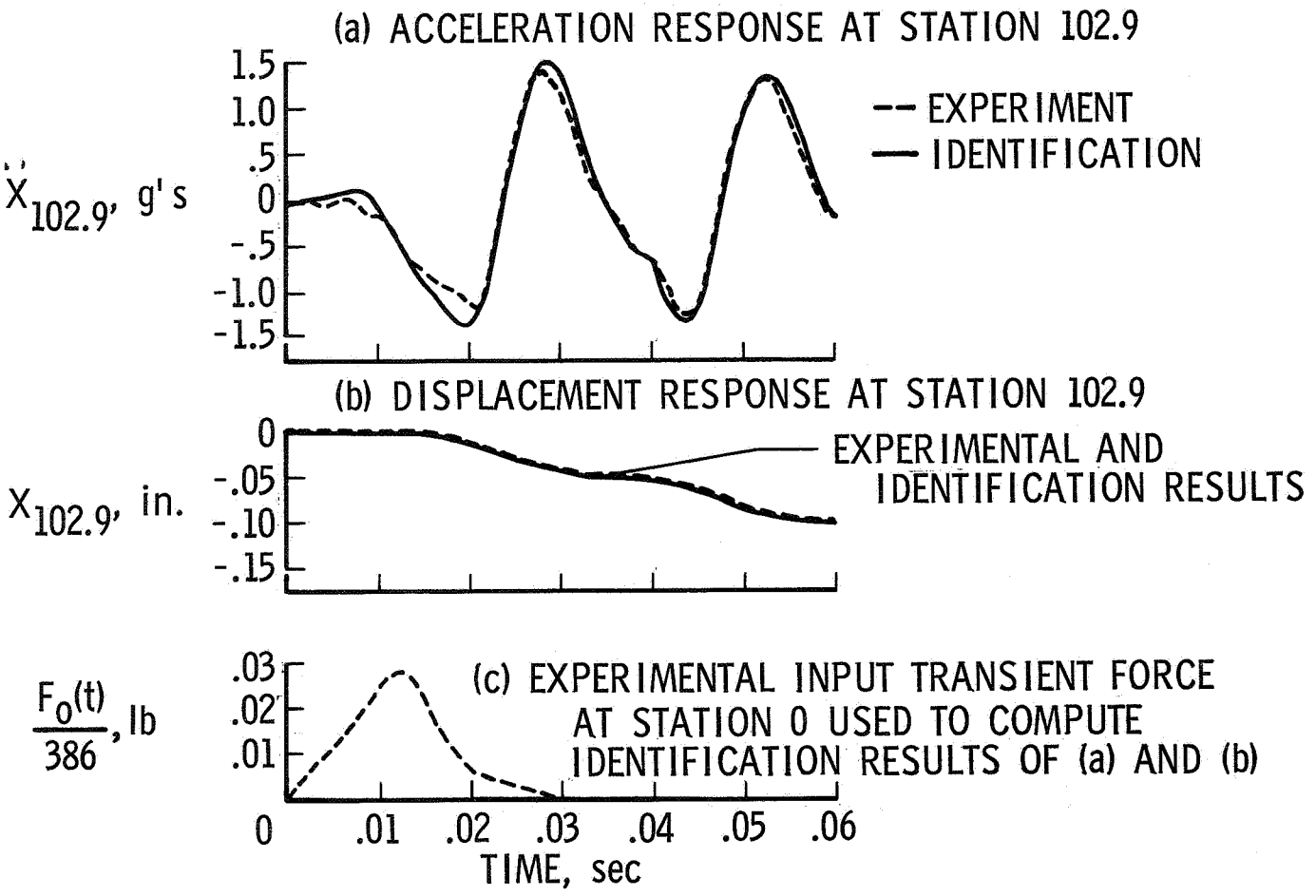


Figure 11.- Comparison of identification and experimental transient response for 1/40-scale model.